Available online at www.sciencedirect.com

SciVerse ScienceDirect

Ceramics International 38 (2012) 3821–3827

CERAMICS INTERNATIONAL

www.elsevier.com/locate/ceramint

Hydration of $Ca_7ZrAl_6O_{18}$ phase

Dominika Madej *, Jacek Szczerba, Wiesława Nocuń-Wczelik, Ryszard Gajerski

AGH University of Science and Technology, Faculty of Materials Science and Ceramics, al. A. Mickiewicza 30, 30-059 Krakow, Poland

Received 28 October 2011; received in revised form 3 January 2012; accepted 12 January 2012
Available online 21 January 2012

Abstract

The hydraulic properties of the $Ca_7ZrAl_6O_{18}$ (C_7A_3Z) phase as well as the hydration products and thermal decomposition mechanism of this hydrated phase were studied. Microcalorimetric analysis has shown that the C_7A_3Z phase reacts with water very quickly, especially in the first 2 h after the start of the experiment. Hydration of calcium zirconium aluminate proceeds with the formation of high refractory calcium zirconate (with melting point 2345 °C), apart from the hydrated, nearly amorphous material. According to the DTA–TG–EGA, FT-IR and SEM/EDS examinations it has been found that not only the hydrates CAH_{10}, C_2AH_8 and C_4AH_{19} are present, but also C_3AH_6 (C = CaO, A = Al_2O_3, H = H_2O), the only hydrated calcium aluminate which is a thermodynamically stable phase above 40 °C. Unhydrated $Ca_7ZrAl_6O_{18}$ and $CaZrO_3$ phases have been found by XRD, but crystalline hydrates have not been detected.

Keywords: B. X-ray methods; B. Microstructure-final; $Ca_7ZrAl_6O_{18}$; Hydration; Unshaped refractories (castables)

1. Introduction

The unshaped refractories (castables), such as refractory mortars and concretes, are more and more commonly used in the production of prefabricated elements and monolithic linings in the heat generation installations. Therefore, the research and development efforts dealing with modern refractory materials technology should be focused on the production and use of these materials.

In these technologies, the fundamental problem of unshaped materials is finding a compromise between maintaining the hydraulic properties of the binder and increasing the resistance to corrosion and thermal shock of the monolithic materials in the thermal unit operating condition. Other properties of material, such as high refractoriness and strength should be taken into consideration.

Calcium monoaluminate $CaAl_2O_4$ (CA; C = CaO, A = Al_2O_3), with the incongruent melting point at 1602 °C, is the main component of currently produced calcium aluminate cements. Calcium bialuminate $CaAl_4O_7$ (CA_2) with the incongruent melting point at 1750–1765 °C, as well as the $Ca_{17}Al_{14}O_{33}$ ($C_{12}A_7$) phase with the incongruent melting point at 1392–1413 °C are the minor components [1]. Tricalcium aluminate $Ca_3Al_2O_6$ (C_3A) is the component of portland cement, with the highest rate of reaction with water. The hydration of $C_{12}A_7$ is also rather intense, while the reaction of CA and CA_2 with water is rather slow, especially in regards to the latter phase. Calcium aluminate hydrates: CAH_{10}, C_2AH_8 and C_4AH_{19} (C = CaO, A = Al_2O_3, H = H_2O) [2] are the transitory hydration product that transform, very often due to the effect of a higher temperature (>40 °C), into the stable C_3AH_6 hydrogarnet phase and gibbsite AH_3 [3,4], which are the only thermodynamically phases stable in the $CaO–Al_2O_3–H_2O$ system, along with $Ca(OH)_2$ [4].

Recently, the phase composition and microstructure of aluminate refractory castables have been modified by zirconium compounds. They not only improve the refractoriness and corrosion resistance of materials but also increase their resistance to thermal shocks. As it has been reported, calcium zirconium aluminate $Ca_7ZrAl_6O_{18}$ (C_7A_3Z; Z = ZrO_2) is the only zirconium containing the aluminate phase that simultaneously exhibits all the hydraulic properties. This is the only three-component compound in $CaO–ZrO_2–Al_2O_3$ (Fig. 1), with the incongruent melting point at 1550 °C. At this temperature, the $CaZrO_3$ phase starts to form [5].

As it has been already reported [6], the C_7A_3Z phase exhibits hydraulic properties similar to the C_3A cement component. The

* Corresponding author. Tel.: +48 12 617 25 39.
E-mail address: dmadej@agh.edu.pl (D. Madej).

0272-8842/$36.00
doi:10.1016/j.ceramint.2012.01.031

hydrogarnet C_3AH_6 with some amount of hexagonal C_4AH_{19} phase is the hydration product.

2. Experimental

2.1. Materials and methods

Calcium zirconium aluminate $Ca_7ZrAl_6O_{18}$ (C_7A_3Z) was synthesized from a stoichiometric mixture composed of calcium carbonate (Chempur 98.81%), alumina (Acros Organics 99.7%) and zirconia (Merck 98.08%). The mixture was homogenized in a zirconium ball mill for 2 h. Subsequently, the specimens were formed as cylinders with diameter and height of 20 mm. Calcination at 1200 °C was the first step of synthesis. Then the cooled samples were cast and burned at 1500 °C for 30 h.

The phase composition of the synthesized samples was determined with the help of XRD equipment (PANalytical X'Pert Pro MPD). The polished fractures of sinters, produced at 1500 °C, were observed under SEM and analyzed by EDS. The ultra high definition NOVA NANO SEM 200 was used for this purpose. As a next step, the synthesized samples were ground and then their specific surface and grain size distribution was measured by a laser diffraction analyzer (the Master Sizer 2000 Ver. 5.60 apparatus of Malvern (UK)).

Calcium zirconium aluminate (C_7A_3Z), defined by the phase and grain size composition, was subjected to the hydration process in a calorimeter, with a water to solid weight ratio = 0.5. The differential non-isothermal – non-adiabatic calorimeter BMR, constructed in the Institute of Physical Chemistry, Polish Academy of Science in Warsaw, was used. The microstructure of hydrated hardened paste was examined under the scanning electron microscope with the EDS analyzer; the phase composition was determined by XRD. The IR studies in the range 4000–400 cm^{-1} were also carried out with the help of a Fourier BIO-RAD FTS60V spectrometer. The samples were prepared as the KBr pellets. The thermal decomposition of hydrates was investigated by DTA with TG and gas emission EGA, using a SDT 2960 type STA (Simultaneous Thermal Analyzer) of TA Instruments (TG, DTG, DTA, QMA).

3. Results and discussion

3.1. Phase composition and microstructure of C_7A_3Z material

The initial material, sintered at 1500 °C, is approximately the calcium zirconium aluminate $Ca_7ZrAl_6O_{18}$ (C_7A_3Z) monophase with some amount of accessory $CaZrO_3$, enriched in Al, as it has been found by XRD and SEM/EDS (Figs. 2 and 3, spot 1). The SEM observations revealed the presence of well developed calcium zirconium aluminate grains. This was confirmed by the EDS analysis (Fig. 3, spot 2).

3.2. Calorimetric studies of C_7A_3Z sample

The heat of hydration was measured for the ground calcium zirconium aluminate material, whose grain size distribution is characterized by the median ($d_{0.5}$), which corresponds to 29.743 μm diameter (Fig. 4) and the specific surface of 0.475 m^2/g. The sample revealed a rather broad, mono-modal grain size distribution. The hydrating paste was produced at a water to solid weight ratio W/C = 0.5. The rate of heat evolution and total heat evolved vs. time are plotted as Figs. 5 and 6.

These figures show that, the intense reaction of the calcium zirconium aluminate (C_7A_3Z) phase with water occurs immediately after mixing. A very high first peak appears, followed by the so-called induction period, between the 2nd

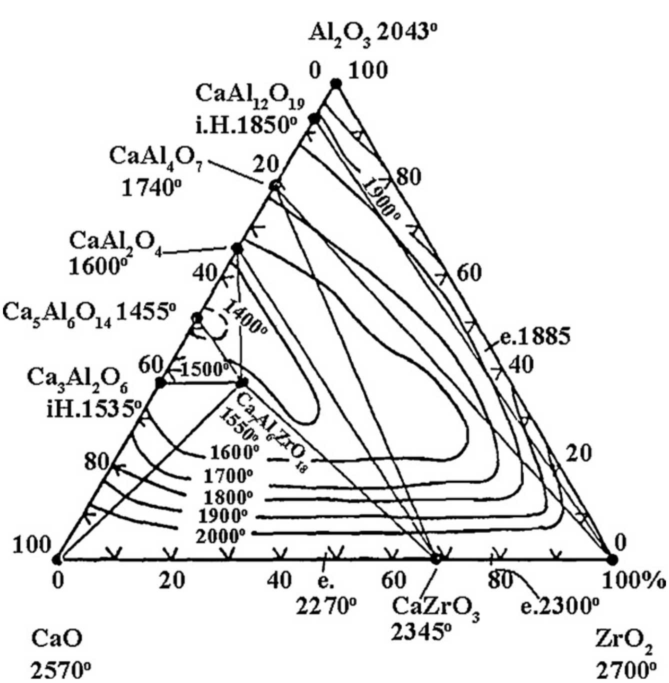

Fig. 1. Diagram of the $CaO–ZrO_2–Al_2O_3$ system [5].

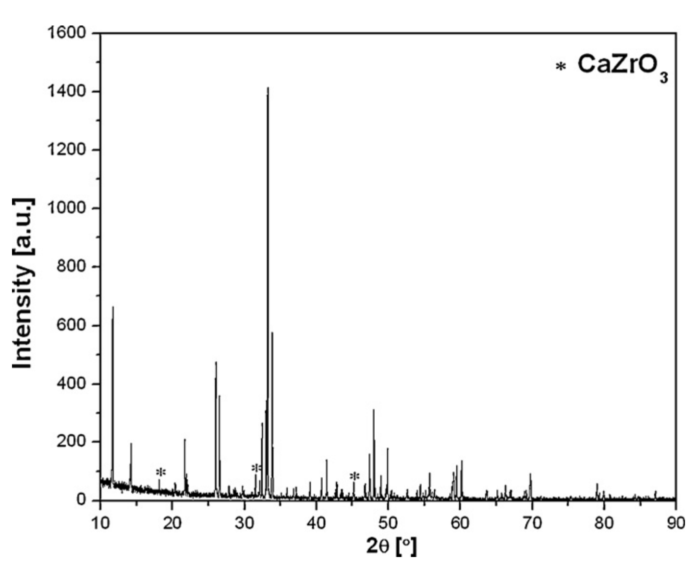

Fig. 2. The XRD pattern of the C_7A_3Z sample after 30-h sintering at 1500 °C; $CaZrO_3$ impurity marked with an asterisk (*).

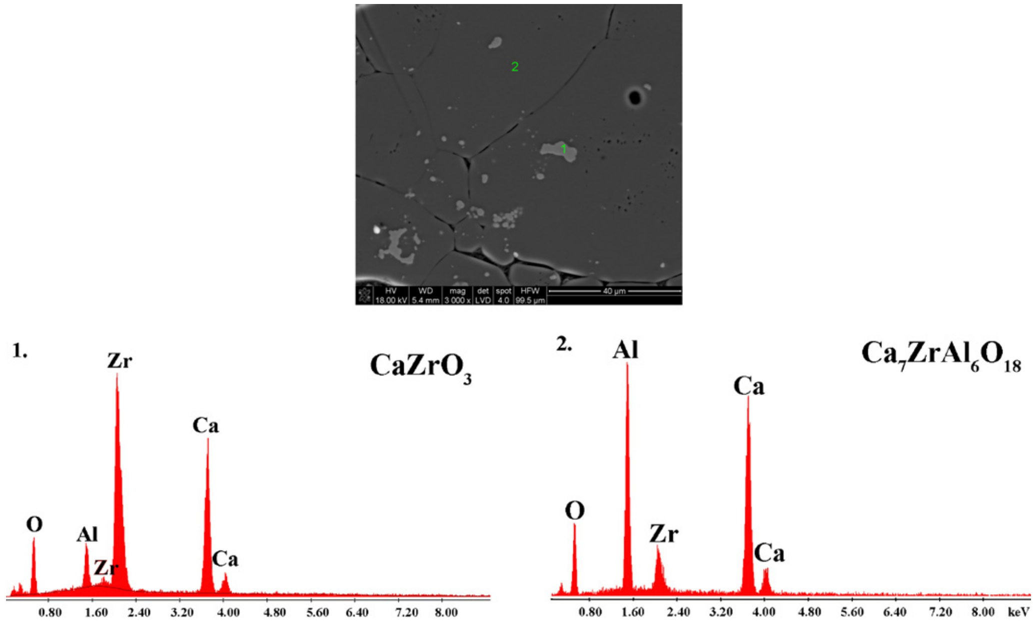

Fig. 3. SEM image of the C_7A_3Z sample microstructure after 30 h of sintering at 1500 °C. (Spots 1 and 2) EDS analysis: 1 – $CaZO_3$ and 2 – C_7A_3Z.

and 8th hour of the process, when the surface of the hydrating grains is covered with transitory products. After this, the hydration is renewed, with a low, broadened second heat effect, due to the crystallization of hydrates and the formation of C_7A_3Z/water contacts. After approximately 18 hrs, the rate of heat evolution decreases due to the slow diffusion controlled hydration process [7]. Therefore, it can be concluded that the course of heat evolution during the C_7A_3Z phase hydration is similar to that of the typical, standard cement pastes. Nevertheless, the proportions between particular stages are different [7].

Therefore, it can be concluded that the hydration process of calcium zirconium aluminate $Ca_7ZrAl_6O_{18}$ (C_7A_3Z) is rather intense, with heat emission accompanying the dissolution of the initial phase and precipitation of hydration products during the first 2 h. After 8 h, the heat emission is significantly slowed down due to the formation of hydrates acting as a membrane separating the unhydrous material from the contact with the liquid phase.

3.3. DTA–TGA–EGA investigation of C_7A_3Z after hydration

The DTA–TGA–EGA measurements show that the dehydration of calcium zirconium aluminate occurs in several steps. There are five temperature maxima in which water is emitted from the sample: 88.43 °C, 159.78 °C, 261.67 °C, 439.20 °C and 534.35 °C, respectively (Figs. 7 and 8). At 88.43 °C, the

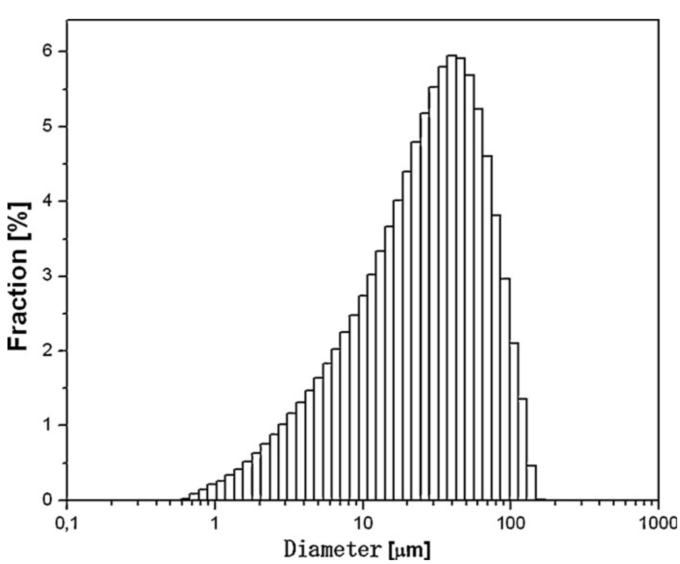

Fig. 4. The particle size distribution in the C_7A_3Z powder sample.

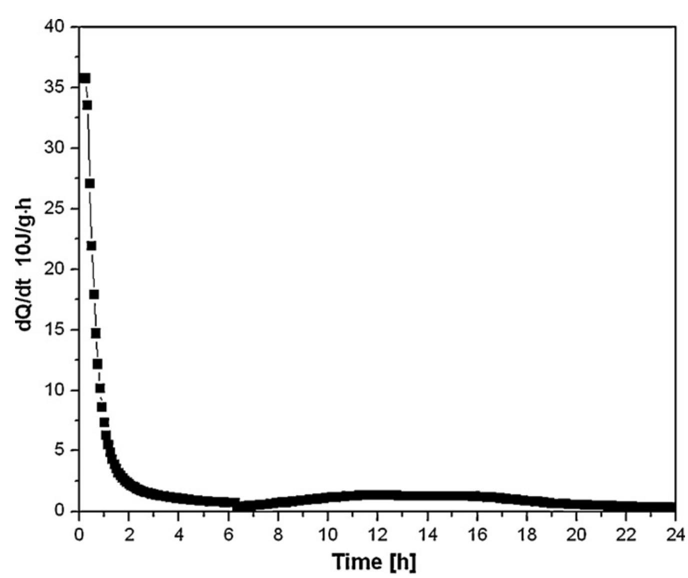

Fig. 5. Microcalorimetric curve illustrating the rate of heat evolution during the C_7A_3Z phase hydration as a function of hydration time.

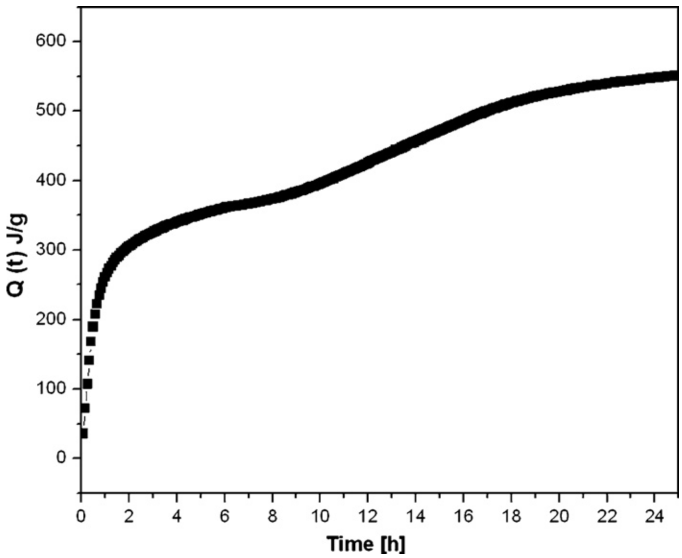

Fig. 6. Heat evolved vs. time for C_7A_3Z hydrated phase.

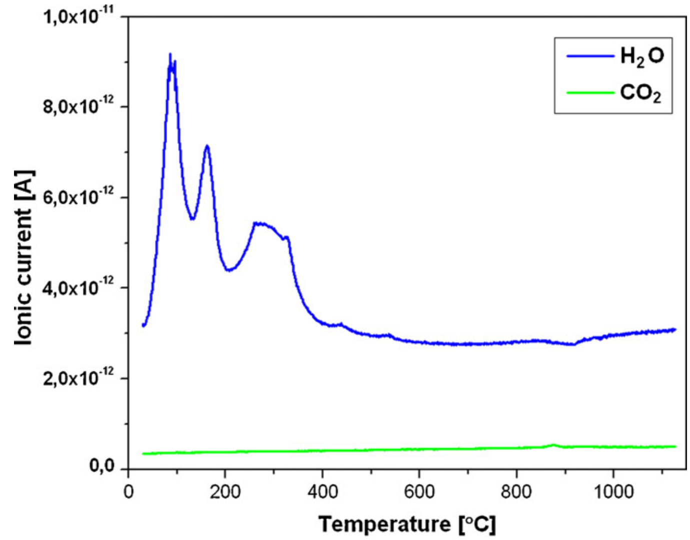

Fig. 8. EGA curve of C_7A_3Z hydrated paste.

first step of hydrated paste decomposition is accompanied by a sharp endothermic DTA peak (Fig. 7) and a 6.85% mass loss as shown by the thermogravimetric curve (Fig. 7). This could be attributed to the dehydration of CAH_{10}, which has been reported by Guirado et al. [8], as well as to the decomposition of AH_3 gel, as reported by George [9]. The CAH_{10} phase dehydration during heating takes place with a low rate at 37 °C and 99 °C and the decomposition of aluminum oxide occurs at 112 °C, respectively [8,9]. Presumably, in the DTA–TGA–EGA measurement conditions, the superposition of peaks occurs.

The second endothermic peak at 159.78 °C also relates to the loss of water (see the EDG curve – Fig. 8) and corresponds to the 6.36% mass loss as shown by the TGA curve. According to Das et al. [10], the above-mentioned peak denotes further dehydration of CAH_{10}. On the other hand, according to George [9], this temperature is close to the characteristic temperature of C_2AH_8 hydrate decomposition. Therefore, it can be concluded that the presence of these two hydrates cannot be excluded.

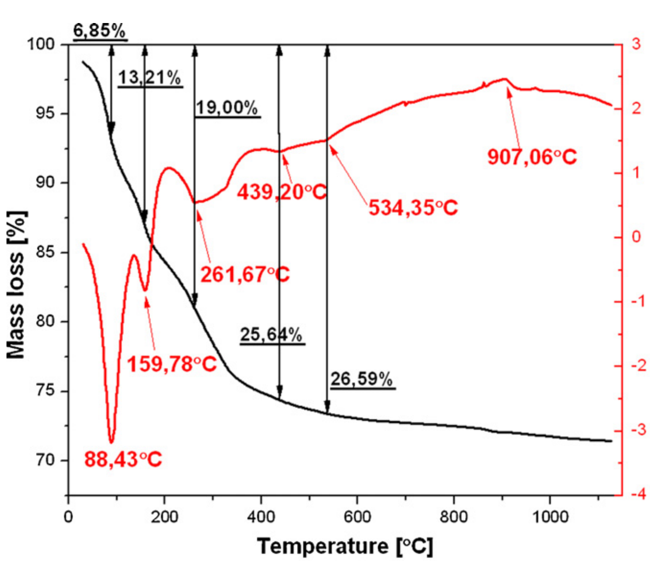

Fig. 7. DTA–TGA curves of C_7A_3Z hydrated paste.

In the third step, water is removed from hydrated C_7A_3Z paste in the temperature range with a maximum at 261.67 °C. This peak is accompanied by a 5.79% mass loss (Fig. 7). According to Das et al. [10], dehydration of C_2AH_8 takes place, or, according to Cardoso et al. [11], C_3AH_6 decomposes.

Two further stages of dehydration in the temperature ranges with maxima at 439.20 °C and 534.35 °C correspond to the 6.64% and 0.95% mass loss, respectively. The first one, according to Radwan and Heikal [2], relates both to the C_3AH_6 and C_4AH_{19} phase decomposition. The second one, on the other hand, relates to the calcium hydroxide dehydration. There is an exothermic peak at 907.06 °C, presumably corresponding to the crystallization of $C_{12}A_7$ or CA. There is no endothermic peak which could be attributed to the decarbonation of the hydrated aluminate sample after inevitable exposure to carbon dioxide. Presumably, this peak coincides with the exothermic one. However, the CO_2 evolution was detected by EGA (Fig. 8).

3.4. XRD studies of C_7A_3Z hydrated paste

Two crystalline components of the hydrated C_7A_3Z paste were found by XRD: initial unhydrated material, i.e. calcium zirconium aluminate $Ca_7ZrAl_6O_{18}$, and calcium zirconate $CaZrO_3$. Crystalline hydrates were not detected. Therefore, it can be concluded that a side effect of C_7A_3Z phase hydration is the separation of calcium zirconate, which is result confirmed by the increased intensity of $CaZrO_3$ peaks in the hydrated sample. In the initial, unhydrated material this zirconate occurs in a negligible amount, and can be treated as an impurity. The relative intensity of $CaZrO_3$ peak corresponding to $d = 2.83586$ in the C_7A_3Z sample was 5.08% before hydration (Fig. 2). It rose up to 43.42% after hydration (Fig. 9). The hydrates, not found in the XRD pattern, appear as an amorphous substance (see higher background). Still some small crystalline phases, confirmed as diffuse XRD peaks, seem to appear.

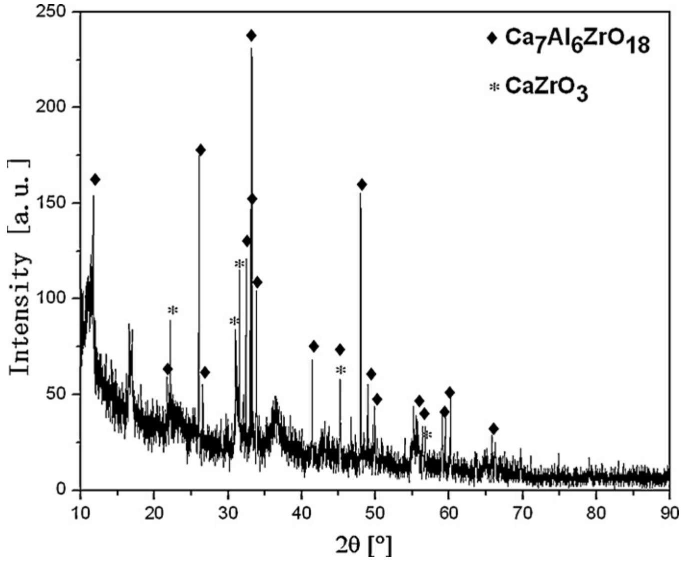

Fig. 9. The XRD pattern of the C_7A_3Z sample after hydration.

3.5. SEM/EDS observations of C_7A_3Z hydrated paste

The SEM/EDS observations of fractured C_7A_3Z samples after hydration reveal the presence of hexagonal calcium aluminate hydrate, presumably CAH_{10} and C_2AH_8 (Fig. 10). The oval calcium zirconate crystals, surrounded by an amorphous, compact material (Fig. 11a and b) can also been seen.

3.6. FT-IR studies of the C_7A_3Z before and after hydration

The FT-IR spectra of the calcium zirconium aluminate phase before and after hydration are shown in Figs. 12–14. From the analysis of the positions of particular bands some conclusions concerning the phase composition and hydration mechanism of C_7A_3Z can be drawn.

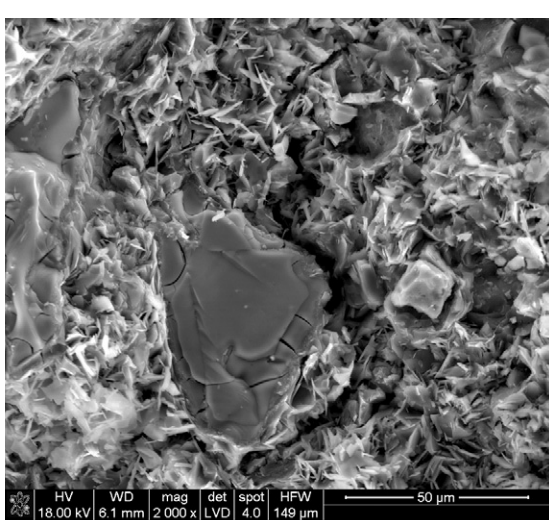

Fig. 10. SEM image of the hydrated C_7A_3Z microstructure. In the center a large nonhydrated C_7A_3Z grain surrounded by the hydrated phases is visible.

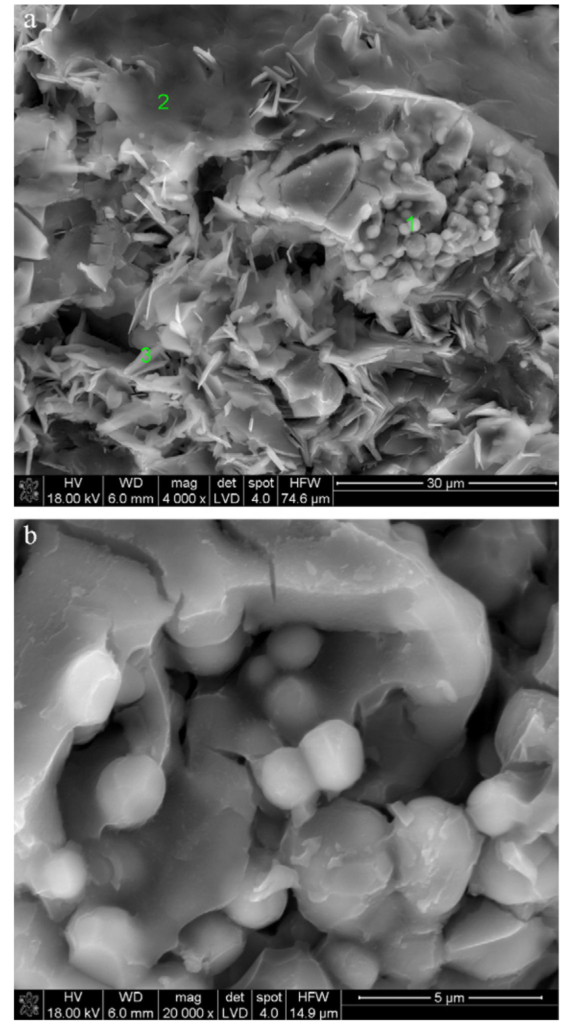

Fig. 11. (a) SEM image of the hydrated C_7A_3Z microstructure: 1 – $CaZrO_3$, 2 – amorphous hydrates, 3 – plate-like hydration products of C_7A_3Z phase. (b) SEM image of the hydrated C_7A_3Z microstructure. Oval $CaZrO_3$ crystals surrounded by the amorphous hydrates.

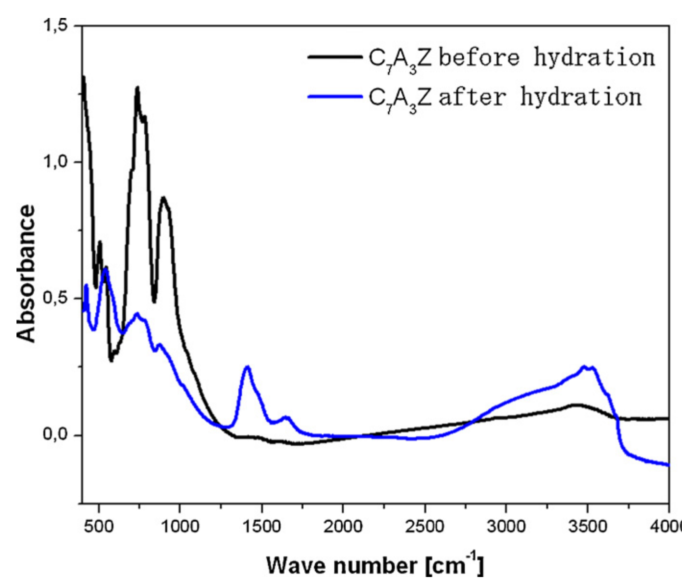

Fig. 12. FT-IR spectrum of C_7A_3Z before (black line) and after hydration (blue line) in the range of 400–4000 cm^{-1}.

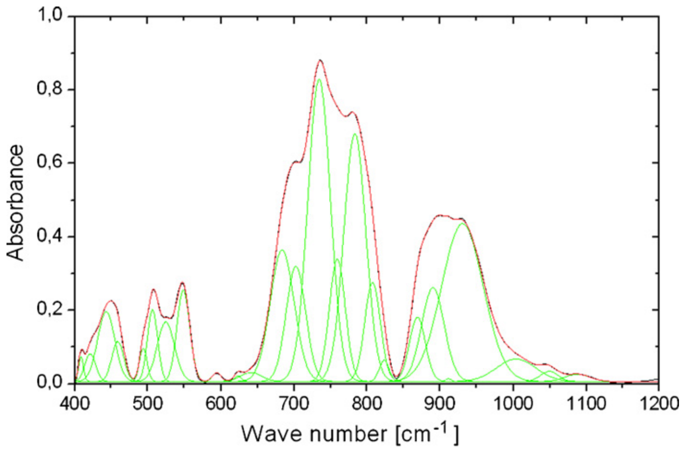

Fig. 13. Decomposition of FT-IR spectrum of C_7A_3Z sample before hydration.

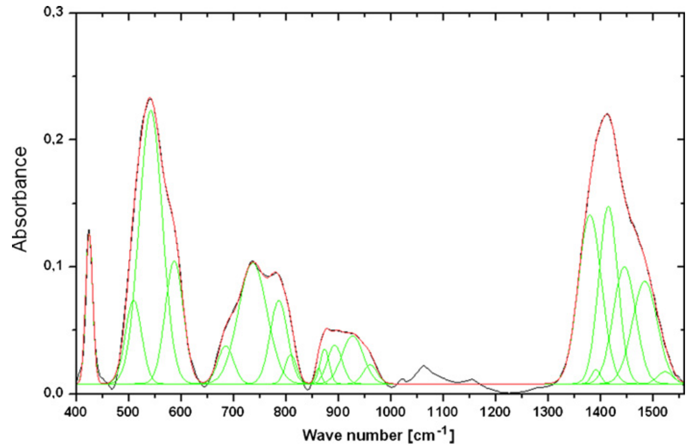

Fig. 14. Decomposition of FT-IR spectrum of hydrated C_7A_3Z sample.

The calcium zirconium aluminate reveals very strong IR absorption spectra corresponding to the wave numbers 443, 684, 703, 735, 759, 783, 808, 890 and 931 cm^{-1}. As the hydration brings about the decomposition of this phase, the intensity of bands attributed to the C_7A_3Z phase decreases and the weaker ones disappear completely (see Table 1). From the FT-IR analysis the following hydration products are confirmed: calcium aluminate hydrates, not only CAH_{10} and C_2AH_8, but also the hydrogarnet C_3AH_6 and gibbsite AH_3. Therefore, the complex course of dehydration curve can be explained. Finally, dehydration leads to the formation of $CaZrO_3$ with high refractoriness.

The bands in the range of 972–3645 cm^{-1} in the FT-IR spectrum are attributed to the calcium aluminate hydrates [16].

Table 1
IR measurements – absorption bands of C_7A_3Z and hydrated C_7A_3Z and the identified phases.

C_7A_3Z before hydration (cm^{-1})	Phase	C_7A_3Z after hydration (cm^{-1})	Phase
409	C_7A_3Z	–	–
421	$CaZrO_3$ [12]	424 ↑	$CaZrO_3$ [12]
443, 459, 494	C_7A_3Z	–	–
506	C_7A_3Z	509 ↓	C_7A_3Z
524	C_7A_3Z	–	–
549	$CaZrO_3$ [12]	542 ↑	$CaZrO_3$ [12]
		587 +	Hydrates [13]
594, 641, 623	C_7A_3Z	–	–
684	C_7A_3Z	685 ↓	C_7A_3Z
703	C_7A_3Z	–	–
735	C_7A_3Z	736 ↓	C_7A_3Z
759	C_7A_3Z	–	–
783	C_7A_3Z	786 ↓	C_7A_3Z
808	C_7A_3Z	809 ↓	C_7A_3Z
823	C_7A_3Z	–	–
		861 +	C_2AH_8 [14]
869	C_7A_3Z	873 ↓	C_7A_3Z
890	C_7A_3Z	892 ↓	C_7A_3Z
911	C_7A_3Z	–	–
931	C_7A_3Z	926 ↓	C_7A_3Z
		960 +	AH_3 [15]
1004, 1049, 1088	C_7A_3Z	–	–
		1379 +	
		1391 +	C_2AH_8 [14]
		1414 +	C_2AH_8 [14]
		1444 +	Carbonates + $Ca(OH)_2$ [2]
		1484 +	Carbonates +$Ca(OH)_2$ [2]
		1522, 2740, 2851, 2926, 3008, 3086, 3215, 3382 +	Calcium aluminate hydrates
		3461 +	Gibbsite [15]
		3530 +	Gibbsite [15]
		3619 +	Gibbsite [15]
		3644 +	$Ca(OH)_2$ [16]
		3669 +	C_3AH_6 [15]

In the C_7A_3Z hydrated sample the gibbsite phase was identified by the presence of 3461, 3530 and 3619 cm^{-1} bands. According to Fernández-Carrasco and Vázquez [15], the bands attributed to gibbsite were 3465, 3525 and 3620 cm^{-1}. The presence of AH_3 suggests the transformation of unstable calcium aluminate hexagonal hydrates into the C_3AH_6 stable hydrogarnet. This is proven by the occurrence of a 3669 cm^{-1} band, which is almost the same as the value found in the literature (3665 cm^{-1}) [15]. It has been reported by Radwan and Heikal [2] that there is a band of $Ca(OH)_2$ in the vicinity of 3640 cm^{-1}. Bands in the range of 1420–1480 cm^{-1} (Feldman et al. [17]) can be attributed to the secondary calcium carbonate, as a result of CO_2 chemisorption. The 1411 and 1390 cm^{-1} bands was attributed to the metastable C_2AH_8 phase (Matusinović et al. [14]). Therefore, this phase was identified by the 1414 and 1391 cm^{-1} bands. The similar wave number values of the C_2AH_8 and CAH_{10} phases [13] make it difficult to differentiate between them.

4. Conclusions

The rapid reaction of calcium zirconium aluminate with water is not convenient due to the low thermal conductivity of concrete. The accumulation of heat during hydration can cause thermal stresses, which in turn, can cause cracks as their values overcome the strength of the hardened material at an early age. The studies of C_7A_3Z hydration reveal that the calcium aluminate hydrates are formed as hydration products. These products are not only the ''low temperature'' hexagonal phases, such as CAH_{10}, C_2AH_8 and C_4AH_{19}, but also the thermodynamically stable hydrogarnet C_3AH_6. All the hydrates are amorphous, except for the unhydrous zirconates $Ca_7Al_6ZrO_{18}$ and $CaZrO_3$ that are present in the paste as crystalline phases, as detected by XRD. The effective reaction of C_7A_3Z with water can be taken into account when discussing the use of this phase as a component of refractory concrete. It is also important that the zirconate phase with high refractoriness (with melting point T_t = 2345 °C) is separated from the C_7A_3Z material during hydration, so that the C_7A_3Z phase can be examined in order to produce a supplementary cementing refractory material capable of accelerating and increasing refractoriness.

Acknowledgements

The financial support of Polish Ministry of Science and Education is acknowledged (Grant No. N N507 457 637).

References

[1] J. Szczerba, Modified magnesia refractories, Ceramika 99 (2007) (in Polish).
[2] M.M. Radwan, M. Heikal, Hydration characteristics of tricalcium aluminate phase in mixes containing β-hemihydate and phosphogypsum, Cem. Concr. Res. 35 (2005) 1601–1608.
[3] B. Pacewska, M. Nowacka, I. Wilińska, W. Kubissa, V. Antonovich, Studies on the influence of spent FCC catalyst on hydration of calcium aluminate cements at ambient temperature, J. Therm. Anal. Calorim. 105 (2011) 129–140.
[4] W. Kurdowski, Chemistry of Cement and Concrete, PWN, Warszawa, 2010 (in Polish).
[5] A.S. Berezhnoi, R.A. Kordyuk, Melting diagram of the system CaO–Al_2O_3–ZrO_2, Dopov. Akad. Nauk URSR 10 (1963) 1344–1347.
[6] K. Fukuda, T. Iwata, K. Nishiyuki, Crystal structure, structural disorder, and hydration behavior of calcium zirconium aluminate, $Ca_7ZrAl_6O_{18}$, Chem. Mater. 19 (2007) 3726–3731.
[7] W. Nocuń-Wczelik (Ed.), Laboratory of Binding Materials, UWN-D AGH, Kraków, 2003 (in Polish).
[8] F. Guirado, S. Gali, J.S. Chinchon, Thermal decomposition of hydrated alumina cement (CAH_{10}), Cem. Concr. Res. 28 (1998) 381–390.
[9] C.M. George, Industrial alumina cement, in: P. Barnes (Ed.), Structure and Performance of Cement, Applied Science, London, 1983.
[10] S.K. Das, A. Mitra, P.K. Das Poddar, Thermal analysis of hydrated calcium aluminates, J. Therm. Anal. 47 (1996) 765–774.
[11] F.A. Cardoso, D.M.M. Innocentini, M.M. Akiyoshi, V.C. Pandolfelli, Effect of curing time on the properties of CAC bonded refractory castables, J. Eur. Ceram. Soc. 24 (2004) 2073–2078.
[12] V.M. Orera, C. Pecharromán, J.I. Peña, R.I. Merino, C.J. Serna, Vibrational spectroscopy of $CaZrO_3$ single crystals, J. Phys. Condens. Matter 10 (1998) 7501–7510.
[13] M.A. Trezza, A.E. Lavat, Analysis of the system $3CaO{\cdot}Al_2O_3$–$CaSO_4{\cdot}2H_2O$–$CaCO_3$–H_2O by FT-IR spectroscopy, Cem. Concr. Res. 31 (2001) 869–872.
[14] Hrvatski skup kemičara i kemijskih inženjera: knjiga sažetaka/Rapić, Vladimir; Rogošić, Marko (Ed.). - Zagreb: Hrvatsko društvo kemijskih inženjera i tehnologa, Opatija, Hrvatska, 24-27.04.2005.
[15] L. Fernández-Carrasco, E. Vázquez, Reactions of fly ash with calcium aluminate cement and calcium sulphate, Fuel 88 (2009) 1533–1538.
[16] V.K. Singh, S.D. Khathri, R.K. Singh, Acrylonitrile Monomer Modified Cement Products, in: 12th International Congress on the Chemistry of Cement, Department of Ceramic Engineering, Institute of Technology, Banaras Hindu University, Varanasi, India, 2007.
[17] R.F. Feldman, V.S. Ramachandran, P.J. Sereda, Influence of $CaCO_3$ on hydration of $3CaO{\cdot}Al_2O_3$, J. Am. Ceram. Soc. 48 (1) (1965) 25–30.